Received: 18 December 2017 | Revised: 10 April 2018 | Accepted: 9 June 2018

DOI: 10.1111/cid.12651

WILEY

ORIGINAL ARTICLE

The micromechanical behavior of implant-abutment connections under a dynamic load protocol

Holger Zipprich Dipl-Ing | Paul Weigl DMD | Christoph Ratka DMD | Bodo Lange DMD | Hans-Christoph Lauer DMD, PhD

Department of Prosthodontics, School of Dentistry, Johann-Wolfgang Goethe University, Frankfurt, Germany

Correspondence
Dr Paul Weigl, Department of Prosthodontics, School of Dentistry, Johann-Wolfgang Goethe University, Theodor-Stern-Kai 7, 60590 Frankfurt, Germany.
Email: weigl@em.uni-frankfurt.de

Abstract

Background: The implant-abutment connection (IAC) is known to be a key factor for the long-term stability of peri-implant tissue.

Purpose: The aim of the present in vitro study was to detect and measure the mechanical behavior of different IACs by X-ray imaging.

Materials and Methods: A total of 20 different implant systems with various implant dimensions and IACs (13 conical-, 6 flat-, and 1 gable-like IAC) have been tested using a chewing device simulating dynamic and static loading up to 200 N. Micromovements have been recorded with a high-resolution, high-speed X-ray camera, and gap length and gap width between implant and abutment have been calculated. Furthermore, X-ray video sequences have been recorded to investigate the sealing capacity of different IACs.

Results: Out of the 20 implant systems, eight implant systems with a conical IAC showed no measurable gaps under static and dynamic loading (200 N). By contrast, all investigated implant systems with a flat IAC showed measurable gaps under dynamic and static loading. X-ray video sequences revealed that a representative conical IAC had sufficient sealing capacity.

Conclusion: Within the limits of the present in vitro study, X-ray imaging showed reduced formation of microgaps and consecutive micromovements in implants with conical IAC compared to flat IACs.

KEYWORDS

contamination, cyclic load, dynamic load, fatigue, implant-abutment connection, microleakage, micromovement, static load

1 | INTRODUCTION

The anchoring of dentures with implants has in the past decades become a accepted and established therapeutic method to treat tooth loss worldwide. There is evidence in the literature that the osseointegration of implants is highly reliable and produces good long-term results.[1,2] Optimized implant surfaces and improved surgical techniques for implant placement ensure a successful and long-term stable osseointegration of the implants after placement.[3] Maturation of the bone in the implant-contact zone allows constant load-dependent adaptation and renewal of the trabecular structure, anchoring the implant, and ensuring proper long-term functioning.

After successful osseointegration and prosthetic loading, the loading force exerted on single-crown implants increases over time, especially in the posterior region of the mouth.[4,5] The increased and cyclical loading induced by the act of chewing also affects not only the implant-bone interface, but also the connection between the implant and the abutment. Compound components may fatigue as quickly as integral components with identical dimensions under cyclical loading, resulting in loosening or fracture of the connection component, which usually occurs long before the failure of the implant material.[6] Furthermore, connections that are initially tight may eventually leak because of an unfavorable angle between components. Furthermore, a high amount of applied load vector can lead to elastic deformations that create a gap in the interface between the abutment and the implant.[7] The gap allows fluid infiltration into the interior of

Holger Zipprich and Paul Weigl contributed equally to this study.

the coupling and the adjoining peri-implant area. The fluid in the interior of the coupling becomes highly contaminated with endotoxins, acidic compounds, and bacteria.[8] Contamination of the peri-implant tissue should be avoided to prevent tissue damage or loss. The aim of this in vitro study was to characterize the mechanical behavior of different implant-abutment connections (IACs) under dynamically increasing and decreasing loads using X-ray imaging.

2 | MATERIALS AND METHODS

The present in vitro study examined 20 different IAC systems in the department of Prosthodontics, School of Dentistry, Johann-Wolfgang Goethe University, Frankfurt/Main, Germany, according to a well-established study protocol. Investigated implants were chosen to obtain a representative selection of IACs (conical/flat connection) and common design characteristics (eg, cone angle, index type). Of the 20 implant systems, the IAC was conical in 13 systems, flat in six systems, and gable-like in one system (Table 1). Implant-anchored single-tooth restorations in the molar region were simulated to investigate the differences between the various IAC types under methodical, induced distortion. The experiments have been performed by the authors H.Z., C.R., and B.L. in main responsibility. P.W. and H.-C.L. served as consultants and supervisors.

2.1 | Simulation of the endosseous implant anchorage, abutment assembly, and single crown restoration

Five implants were tested per implant system. Test implants were each embedded in a T-shaped block of resin (Technovit 4004; Heraeus Kulzer GmbH Division Technology, Wehrheim, Germany; total height = 24.0 mm; horizontal bar height = 14 mm; horizontal bar width = 10 mm; vertical bar height = 10 mm; vertical bar width = 20 mm, depth = 10 mm). Using a muffle and an alignment tool, each implant was embedded in an identical position within the resin. Each implant was embedded so that the platform was 3 mm above the surface of the resin block, in accordance with DIN EN ISO 14801:2016 standards.

Straight abutments were mounted on the implants using the torque recommended by the manufacturers (Table 1). Toa void bias, a precalibrated universal torque wrench (Torsion Meter 760, Stahlwille, EDUARD WILLE GmbH & CO KG, Wuppertal, Germany) was used to mount all abutments instead of the torque wrenches provided by the implant manufacturers.

To achieve comparable results independent of abutment designs, the abutment diameter was reduced to 3.45 mm using a lathe (EMCOTURN 120; Controller TRONIC TM02; EMCO Maier GmbH, Hallein-Taxach, Austria) and, if necessary, the length was shortened occlusally. The lathed surface was sandblasted with alumina particles (110 μm, 2.5 bar). A threaded sleeve (M5 × 0.5 mm) was cemented onto each lathed abutment (NimeticTM Cem; 3M Espe, Seefeld, Germany), creating a cement gap of 0.05 to 0.1 mm between the sleeve and the abutment. A metal ball with an outer diameter of 8.0 mm was screwed onto the threaded sleeve. The force-introduction center (ie, the center of the ball) was precisely positioned 8.0 mm above the implant platform.

2.2 | Simulation of dynamic chewing forces

The resin block with the embedded implant was clamped into a two-dimensional chewing simulator with two separately controllable, simultaneously acting electrodynamic actuators standing perpendicularly to one another (Figure 1A,B). The actuators worked on the moving coil principle to generate a force vector freely adjustable in angle (– 0° to + 90°) and magnitude (0-300 N) on the IAC (Figure 2A,B). The amount and direction of the chewing-force vector resulted from vector addition of the forces provided by the two actuators. The power of the two actuators was calibrated using three orthogonally aligned force sensors (HBM U2B 500N; Hottinger Baldwin Messtechnik GmbH, Darmstadt, Germany).

The maximum force of each simulated chewing cycle was increased by 25 N over eight consecutive test cycles, starting at 25 N and ending at 200 N. A dynamic load was placed on the force ball to simulate the biomechanical situation of chewing in the posterior region of the mouth according to the DIN 14801:2016 standards. The loading of the implants can be described in three phases (Figure 3):

In the first phase, a force was generated in the vertical (axial) direction by the vertical actuator (Figure 1A, no. 1) starting at 0 N and increasing to the maximum force for the cycle at a slew rate of 0.3 N/ms (phase 1, Figure 3).

In the second phase, the force of the horizontal actuator (Figure 1A, no. 2) was activated and the horizontal force was increased while the vertical force was reduced. The increasing horizontal force and decreasing vertical force were balanced, so that the magnitude of the resulting force vector was kept constant at the level of maximum force. This increase in horizontal force and decrease in vertical force rotated the direction of the resulting force vector from vertical to 30° from vertical. This was performed over the same time interval as that required to reach the maximum force in phase 1.

During the transition from phase 2 to phase 3, a static load was maintained for 5 seconds. This was used to compare the behavior of the IAC between static- and cyclical-loading situations.

In the third phase, the 30° inclination of the applied force vector was kept constant, while the magnitude of the force was reduced at a rate of 0.6 N/ms until it reached 0 N (phase 3, Figure 3).

2.3 | Analysis of the IAC

The behavior of the IACs under cyclic loading was analyzed using sequential two-dimensional radiographs (Figure 4) collected on an FXS 160.50 X-ray system with an X-FXT-160.45 X-ray bulb (Feinfokus, Germany). The X-ray parameters could be adjusted and combined from 10 to 160 KV and from 0.01 to 1 mA to obtain the best possible representation of the IAC. X-ray images were amplified using a Thales TH 9438 QX (Thales Group, Neuilly-Sur-Seine, France). Consecutive, intensified X-ray images were recorded using a high-speed digital camera (Redlake MotionPro HS-3; IS-Imaging Solutions GmbH, Eningen, Germany) operating at 1000 frames per second and a resolution of 1280 × 1024 pixels in monocolor mode.

TABLE 1 Comparison of all investigated implant systems, including implant dimension, screw torque, connection specification, and gap forming under load and at the maximum force of 200 N

Implant			Implant dimension		Gap size in relation to dynamic load cycle								Connection specifications		IAC behavior at dynamic load cycle 200 N			
Manufacturer	Implant type	Diameter (mm)	Length (mm)	Screw torque (N cm)	25 N (µm)	50 N (µm)	75 N (µm)	100 N (µm)	125 N (µm)	150 N (µm)	175 N (µm)	200 N (µm)	Connection type and angle	Length of load transferring interface (µm)	Gap width (200 N)	Gap length at 200 N (µm)	Ratio gap length/ interface length (%)	Consistency of gap
Argon Dental	K3Pro standard with hex	4.5	13	30	0	0	0	0	0	0	0	0	Cone; α = 1.5°	2620	0	0	0.00	n
Astra Tech	Osseospeed	4.0	11	20	0	0	0	1.2	2.4	3.6	6	12.4	Cone; α = 11°	1260	12.4	305.6	24.25	n
Astra Tech	Osseospeed	4.5	11	25	0	0	0	0	0	0.4	4.8	8	Cone; α = 11°	2310	8	136.8	5.92	n
BEGO	Semados S	4.5	13	30	0	0	0	0	0	0	0	0	Cone; α = 45°	800	0	0	0.00	n
Biodenta	Tissue level RP	4.1	12	35	0	0.4	1.6	3.6	5.2	7.2	8.4	12.4	Cone; α = 7°	Not measurable	12.4	Not measurable	Not measurable	Not measurable
Biodenta	Bone level B2	4.2	14	35	0	0	0	0	0	0	0	0	Cone; α = 6°	2180	0	0	0.00	n
BIOMET 3i	BIOMET 3i	4.0	13	20	3.6	4.8	5.6	5.6	5.6	7.6	8.8	11.6	Flat connection	370	11.6	370	100.00	y
BPI	Bpisys.classic VS	4.1	14	35	4.8	5.6	6	6.8	7.6	8.4	10	11.6	Gable α = 45°	Not measurable	11.6	Full length	100.00	y
Bredent	Bredent	4.5	9	30	0	0	0	0.8	3.2	6	8.4	13.2	Flat connection	650	13.2	650	100.00	y
Camlog	K series	4.3	9	20	0	0.8	2	4	6	8.8	11.2	15.2	Flat connection	350-525	15.2	525	100.00	y
Dentsply Friadent	Ankylos B11	4.5	11	15	0	0	0	0	0	0	0	0	Cone; α = 5.71°	2170	0	0	0.00	n
Dentsply Friadent	XIVE S plus	4.5	13	24	0	0.4	1.6	2.8	4.8	6.4	8	11.6	Flat connection	700	11.6	700	100.00	y
Heraeus	IQ-nect	3.75	13	30	9.2	11.6	14.4	18.8	23.2	28.8	32.5	42	Flat connection	575-770	42	770	100.00	y
Leone	Exacone	4.1	12	30	0	0	0	0	0	0	0	0	Cone; α = 1.5°	3260	0	0	0.00	n
Nobel Biocare	Nobel replace	4.3	13	35	0	0	0.4	0.8	1.2	2.8	3.6	4.8	Flat connection	245-700	4.8	700	100.00	y
Nobel Biocare	Nobel active	4.3	13	35	0	0	0	0	0	0	0	0	Cone; α = 12°	1030	0	0	0.00	n
Osstem	GS III	4.5	13	30	0	0	0	0	0	0	0	0	Cone; α = 11°	1240	0	0	0.00	n
Straumann	Bone level	4.1	12	35	0	0	0	0	0	0	0	0	Cone; α = 15°	720	0	0	0.00	n
Straumann	synOcta and Octa	4.1	12	35&15	0	0	0	1.1	4.2	7.2	12.7	18.6	Cone; α = 8°/45°	765 (45°)	18.6	765	100.00	y
Straumann	Massive abutment	4.8	12	35	0	0	0	0	0	0.4	2.8	5.6	Cone; α = 8°	2340	5.6	532.8	22.77	n

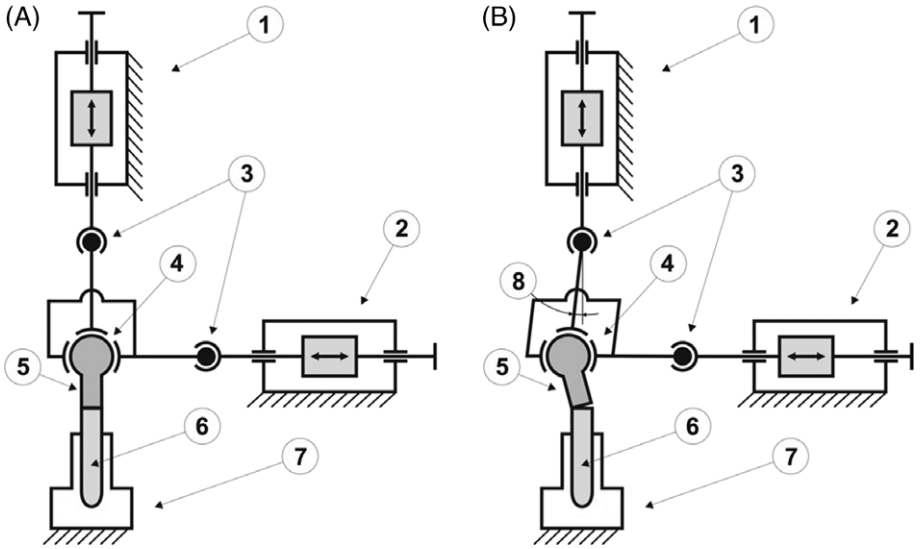

FIGURE 1 Schematic drawing of the setup for cyclic loading of an implant-abutment-joint in the nonloaded phase (A) and (B) in the loaded phase. The instrument components consist of an electro-dynamic actuator generating vertical load (1), an electrodynamic actuator generating horizontal load (2), a rod end (3), a ball head joint (4), an abutment and fixed ball head (5), and the implant (6) embedded in a resin block (7). Rotation due to horizontal shift of the abutment is shown in (8). The force coupling was designed to be flexible enough to avoid uncontrolled shear forces and moments on the force transmission ball. This flexibility was achieved by using swivel heads in the force-introduction strands ([B], no. 3) and in the congruent pans of the force-application sphere ([B], no. 4). (B) A rotation of the force transmission ball relative to the abutment due to the horizontal force component of the load; no. 8 shows the resulting angle of inclination in the vertical force-generating strand

2.4 | Measurement of the gap at the implant-abutment interface

Raw data from the high-speed camera were postprocessed using the graphical programming system LabVIEW version 8.2 (National Instruments, Austin, Texas). The raw data contained a relatively high amount of noise due to the high light sensitivity of the image sensor. To reduce image noise, 11 consecutive individual images were combined to create a single image. The algorithm averaged 11 identically placed pixels from the individual images to create each pixel in a single noise-reduced image. The 11 consecutive images represented a period of 11 ms during cyclic loading with a force increasing at 0.3 N/ms. Therefore, every noise-reduced image included a force increase of 3.3 N during phase 1. During phase 2, the noise-reduced image captured changes in the vector angle depending on the load cycle, which ranged from 0.495° (200 N cycle) to 2.96° (25 N cycle). During phase 3, the averaged image also captured a continuously decreasing load from 6.6 N to 0 N.

Two experienced investigators independently evaluated each of the noise-reduced images and selected the image with the largest gap in the interface or with the largest displacement of the entire test body. These selected images were used for the quantitative analysis. The investigators viewed the images in both dynamic and static

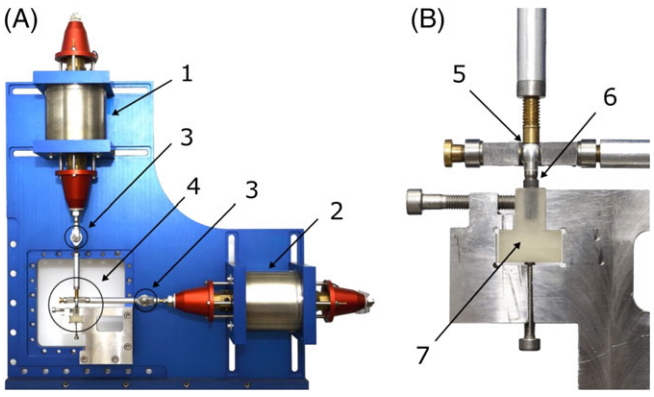

FIGURE 2 Photograph of setup for cyclic loading of the implant-abutment joint. The instrument consists of an electrodynamic actuator generating vertical load (A), and an electrodynamic actuator generating horizontal load (B). An electrodynamic actuator generating vertical load (1), an electrodynamic actuator generating horizontal load (2), a rod end (3), a fixation device for the specimen (4), an abutment and fixed ball head (5), and the implant (6) implant embedded in a resin block (7) are necessary to imitate static and dynamic chewing load

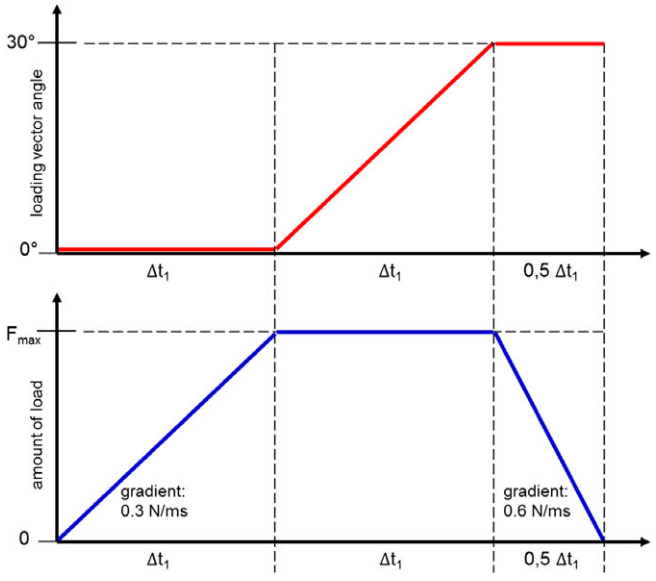

FIGURE 3 Schematic plot of loading vector force and angle throughout a load cycle. After one cycle, the maximal load was increased by 25 N for each subsequent cycle until it reached 200 N

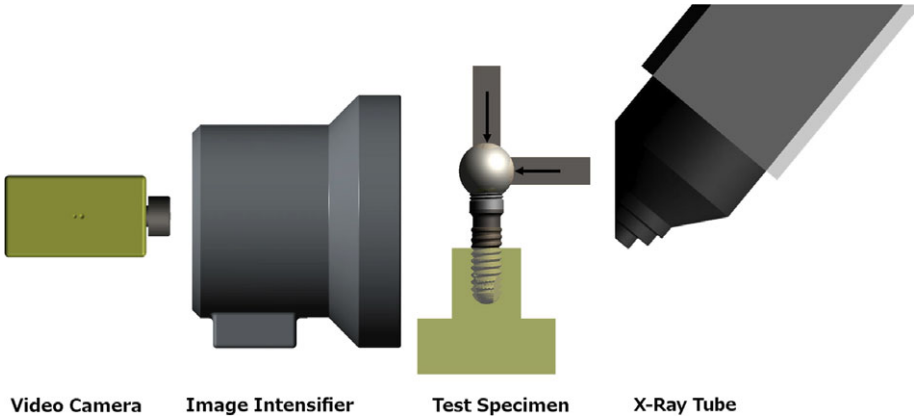

FIGURE 4 Computer-Aided-Design (CAD) rendered schematic plot of the dynamic X-ray imaging device (all parts CAD rendered)

modes to ensure reliable identification of the best representative images.

For the quantitative analysis, the dimensions of the gap were measured at the implant-abutment interface in the selected images using GNU Image Manipulation Program (version 2.8.0; www.gimp.org). The "tape measure" tool in the software was used to determine the number of pixels within the gap. The size of the gap was measured in two dimensions. The gap width (G_W) is the perpendicular distance between the implant and the abutment at the outermost boundary of the implant-abutment interface in relation to the implant axis. The gap length (G_L) is the distance between the beginning of the detectable gap and the outermost boundary of the implant, measured along the surface of the implant.

The gap widths of the five replicated of each implant system were averaged for each maximum force. The gap lengths were also averaged for the five replicates at a maximum force of 200 N. In addition, the length of contact (l_C) at the implant-abutment interface was calculated using the equation $l_C = l_L\text{-}G_L$. The overall length of the implant-abutment interface (l_L) was known.

2.5 | Calibration of the measurement apparatus

The number of pixels was converted into the absolute distance between the abutment and implant in the interface area using the following calibration methods: Two special calibration bodies were used to determine the resolution of the coupled camera, optics, image intensifier, and X-ray bulb. The calibration bodies consisted of a sheet with a rectangular hole substituted for the implant. The hole was evaluated using an optical measuring table from Leitz (Leica Microsystems GmbH, Wetzlar, Germany) and an integrated micrometer head (DIGIMATIC series 350; Mitutoyo Germany GmbH, Neuss, Germany). The rectangular hole was positioned horizontally in one calibration body and vertically in the other. Radiographs of the two calibrating bodies were evaluated as described above, and the dimensions of the rectangles were correlated with the numbers of pixels.

The per-pixel resolution of the X-ray unit was determined at a distance of 1 cm between the center of the calibration body and the beam exit window. The resolution of the horizontally positioned rectangle was calculated to be: 1516 μm (measuring table)/756 pixels = 2.005 μm per pixel. The resolution of the vertically positioned rectangle was calculated to be: 1522 μm (measuring table)/768 pixels = 1.981 μm per pixel. The resolutions in the vertical and horizontal positions were both rounded to 2.0 μm per pixel.

2.6 | Normalization of the radiographs under static versus dynamic load

To compare the static and dynamic loading situations, radiographs were normalized using clearly visible landmarks. The corresponding images of static and dynamic loads were aligned with reference to the external geometry of the implant at the shoulder area.

2.7 | Representative comparison of static and dynamic loads

In order to compare the type IAC under static and dynamic loads, two representative implants were selected. The Ankylos (Ø 3.5 mm; 17 mm length) and CAMLOG (Ø 3.8 mm; 13 mm length) implants were selected as representative implants and were exposed to a maximum load cycle of 200 N. Radiographs were collected before, during, and after applying the static load with 30° displacement. Then, implants were immediately subjected to the dynamic loading protocol with a maximum force of 200 N. Images were recorded using slow-motion video prior to load application, at 200 N and 30° displacement, and again after any load application. Furthermore, a single frame was collected without any load applied. To facilitate visual comparison of the X-ray images, the outermost boundary line of the implant surface at the shoulder area was aligned in each of the images.

2.8 | X-ray video analysis of the sealing capacity

To analyze the clinical relevance of the sealing capacity of the implant-abutment-connection, X-ray sequences of a flat (butt joint) and conical IAC have been recorded. A butt joint with a radiologically detectable microgap and a conical IAC without a radiologically detectable microgap were tested in an artificial gingiva made from Impregum Penta (3M ESPE) with a gingival height of approximately 3.0 mm. An access channel (Ø = 2.0 mm) to the IAC for a radiopaque fluid was placed within the artificial gingiva. The liquid was composed of a saliva substitute (Salivanatura; Parnell Pharmaceuticals) and an X-ray contrast agent

(Imeron 300; Bracco Imaging Germany GmbH, Konstanz, Germany). Video S1 (Supporting Information) gives an overview the IAC together with the access channel filled with radiopaque fluid.

3 | RESULTS

The simulated chewing force resulted in elastic deformation of the implant-abutment specimen, the clamp holding the specimen, and the entire test station. In some cases, the chewing force also caused a gap in the IAC. Each of those deformations resulted in a vertical and horizontal change in the position of the force transmission ball (Figure 1B) relative to its position in the unloaded condition (Figure 1A).

The design of the IAC varied among the 20 investigated implant systems (Figure 5). Thirteen implants with conical connections, six with flat connections, and one with a gable-like connection have been investigated. The averaged gaps at the IAC for each maximum load are listed in Table 1. All implants with a flat connection (BIOMET 3i, Bredent, Camlog K-series, Dentsply Xive S plus, Heraeus iQ-nect, Nobel Biocare-Nobel Replace) and the implant with the gable connection (BPI-bpisys.classic VS) showed measurable gaps between the implant and abutment under both static and dynamic loading. Out of the 13 implants with conical connections, eight implants showed no measurable gap formation under dynamic or static loading (Straumann Bone Level, Osstem GS III, Nobel Biocare-Nobel Active, Leone Exacone, Argon Dental K3 Pro Standard with hex; Bego Semandos S, Biodenta Bone Level B2, Dentsply Ankylos). One implant with a conical connection showed no measurable gap under static loading but an obvious gap under dynamic loading (Biodenta Tissue Level). The remaining four conical connection implant systems showed measurable gaps under both static loading of 200 N and dynamic loading of either 100 N (Dentsply Astra Osseo Speed 4.0, Dentsply Astra Osseospeed 4.5, Straumann synOcta), or 150 N (Straumann massive abutment). The Astra Osseospeed implant system with a diameter of 4.5 mm presented a smaller gap width and length compared with an implant of the same system with a diameter of 4.0 using the same type of conical connection and cone angle.

In the flat IAC systems, a sufficiently strong horizontal force caused a small rotation of the abutment relative to a pivot point on the edge of the implant platform due to clearance between the joined components (Figure 6A). A subsequent reduction of the horizontal load caused a reset of the elastically deformed components (implant, abutment, connecting screw) in implants with a "butt"-style connections. Dynamic loading caused cyclical formation and regression of a gap in the implant-abutment interface.

All of the eight implant systems that did not show gaps under loads had a conical IAC (Table 1, Figure 6B). Little to no abutment rotation was observed when dynamic load was applied to systems with conical interfaces. When relative movement between the abutment and the implant in the conical connection occurred, no radiologically detectable gap at angled surfaces could be observed. Under the conditions tested, differences in the length and angle of the conical connection had no measurable effect on gap formation; however, such differences did affect the extent of radiologically visible movement of the abutment relative to the implant.

The vertical angle error (Figure 1B, no. 8) at 200 N force was detected based on the change in the horizontal position of the loading ball (min: 212 μm with Bego Ø 4.5 mm; max: 536 μm with Astra Tech Ø 4.5 mm). The minimum and maximum vertical angle errors were calculated to be 0.00218° and 0.00536°, respectively. The minimum and maximum horizontal angle errors were determined to be 0.0001° (XIVE with Ø 4.5 mm) and 0.00056° (Leone with Ø 4.1 mm), respectively. Because the maximum resulting angular error was only +0.00508° (Astra Tech with Ø 4.5 mm), no correction of the results using an error algorithm was necessary.

The gap lengths under a dynamic maximum load of 200 N in the 30° direction (Table 1) were used to calculate the implant system-specific contact lengths of the force-transmitting implant-abutment interface regions.

When analyzing the connection specifications of the investigated implant systems, it became obvious that increased gaps seemed to form when the contact length of the implant-abutment interface is rather short. However, even small gap lengths lead to continuity between the peri-implant outer environment and the inner lumen of the implant.

In both conical (Figure 7) and butt connection (Figure 8A,B) implants, static loading caused greater dislocations of the abutments than the dynamic load in the identical experimental setup with the same force vector (200 N, 30°).

For a better understanding and illustration of the present findings, the clinically relevant sealing capacity of representative IACs was visualized. The static and dynamic loading of two types of connections was visualized by compiling slow-motion X-ray movies from sequential radiographs after applying a radiopaque artificial saliva. The recorded sequences clearly show the invasion of the artificial saliva into the flat IAC during a cycle with maximum force of 200 N (Video S2). In contrast, the conical IAC was not penetrated by artificial saliva (Video S3).

4 | DISCUSSION

The 20 implant-abutment systems showed design-dependent behavior when load was applied. Horizontal forces caused a small rotation of the abutment relative to a pivot point on the edge of the implant platform. Conical connections had less radiologically detectable microgap formation at the implant-abutment interface (Figure 6B). Especially, implant systems with a conical IAC showed reduced radiologically detectable microgap. In 8 out of 13 investigated conical connection implant systems, no microgap was obvious, whereas gap formation was detected in all of the six implant systems with a flat IAC.

Similar results regarding the favorable sealing capacity of conical connections were shown previously using real-time radioscopy with synchrotron light sources and using a finite element study, which showed that no microgap occurred in the case of a conical IAC.[9,10]

To avoid misinterpretation, especially with regard to clinical application, it is essential to note that the results of the present in vitro study cannot be transferred one-to-one to the clinic. Loading was performed at up to a force of 200 N. Thus, no statement about a

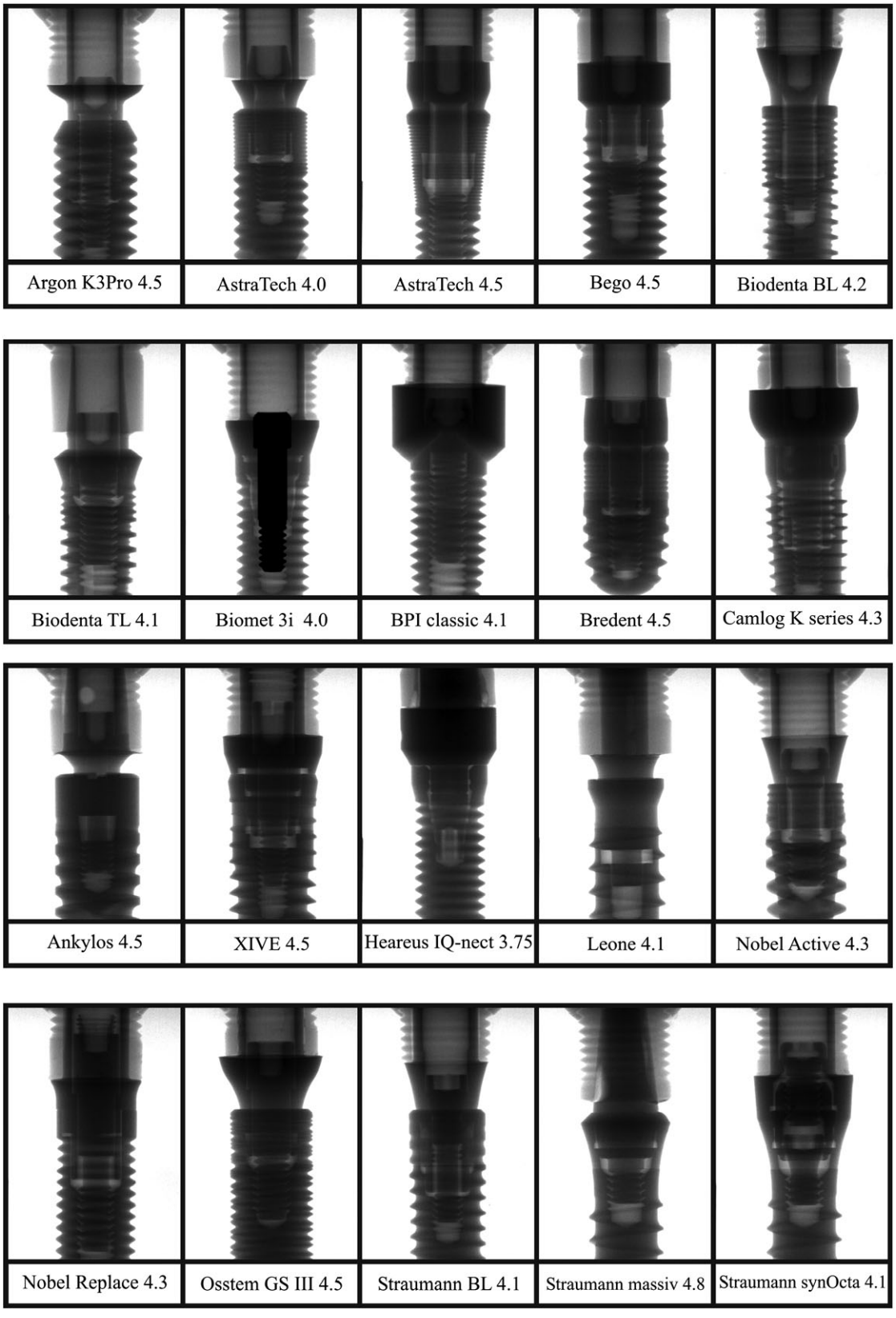

FIGURE 5 Two-dimensional X-ray images of the implant-abutment joint designs of the 20 implant types investigated in the present study (nonloaded)

potential gap formation, also of conical connections, at higher loading forces can be made.

Static, and therefore relatively long acting, horizontal forces were able to cause gaps even at the conical joint surfaces by increased elastic deformation (Figure 7A; Table 1). Design parameters other than the conical versus flat connection design might further influence gap formation. The effective cone length, wall thickness ratios of the implant and the abutment, and the pretensioning of the connecting

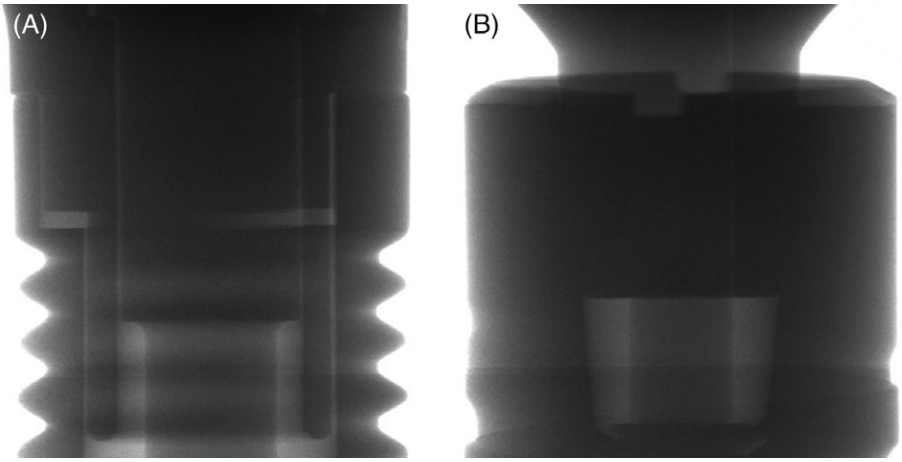

FIGURE 6 Two-dimensional X-ray image of the implant-abutment connection (nonloaded). A, Flat implant-abutment connection with visible clearance gaps. B, Conical implant-abutment connection without visible clearance gaps

screw must be optimally balanced in order to withstand loads of 200 N with 30° directional displacements without gap formation. In addition, manufacturing artifacts, such as the surface quality of the joining surfaces (eg, the cone surface, the screw-head support, and screw thread) and the tolerance of the cone angle, influence the overall quality of the IAC.

Beside the type IAC, the screw torque might also be of particular interest. Each screw was mounted at the torque recommended by the manufacturer (Table 1). Depending on the screw configuration and the tightening torque, a preload is generated that connects the implant and the abutment. The higher the tightening torque, the higher the clamping force between the implant and abutment and consequently the sealing of the IAC. However, the torque is limited by several factors, such as deformation of abutment or implant, that might promote cleft formation and impair primary stability or osseointegration of the implant. Thus, all implant components should be perfectly coordinated to prevent damage to the implant and the patient.

Rack et al tested implant systems using the same type of static load as the present study and imaged their experiments at a high-resolution synchrotron facility. To achieve sufficient image quality with static loading, very long exposure times (up to 10 seconds) were required. This long duration of load might influence the results.[11,12] In the present setting, a shorter exposure time and an equally high dynamic load was applied, leading to a greater dislocation of the abutment relative to the implant platform and thus a larger microgap during the static load of a nonconical abutment connections (Figure 7B). Static loads are considered clinically relevant in the context of chewing or maximum intercuspidation. Static loading plays not only an important role in the investigation of myoelectric activity in masticatory muscles and bit forces,[13,14] but also in the analysis of resistance of different implant-related components against biting forces. Exemplarily, an in vivo measurement of bite forces at posterior implants, applied a comparable range of static loading of up to 200 N as applied in the present study.[15] Furthermore, high values of static loads and maximum biting forces occur in patients with severe bruxism, who are considered a difficult population to treat.

Cyclical gap formation can cause wear on metal surfaces. Titanium and iron remnants were reported to be found in soft-tissue and hard-tissue biopsies retrieved from sites of peri-implantitis sites.[16] However, such reports should be discussed carefully with respect to many possible reasons for contaminations. Furthermore, wear patterns, such as adhesive wear and fretting, were seen in implants after cyclical loading regardless of the interface design.[7] Previous studies investigating a gap formation at the implant-abutment interface based on fluid discharge, as indicated by measures of bacterial contamination, reported that conical connection implants showed improved salivary sealing under load, although the sealing was not absolutely reliable.[17-20] The cyclical opening and closing of the microgap seems

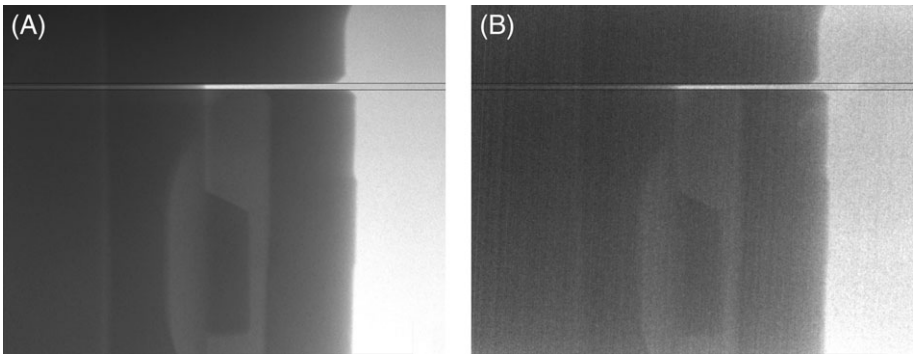

FIGURE 7 Two-dimensional X-ray image of a conical implant-abutment connection. The static load caused enhanced dislocation of the abutment. A, Static load of 200 N at 30°. B, Dynamic loading cycle at 200 N and 30°

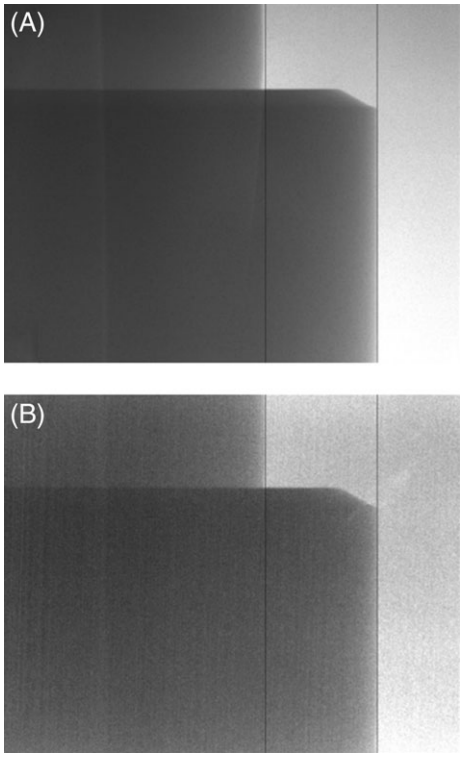

FIGURE 8 Two-dimensional X-ray image of a butt implant-abutment connection. The static load caused an enhanced gap width. (A) Static load of 200 N at 30°. (B) Dynamic loading cycle at 200 N and 30°

to act as a pump, which causes the peri-implant tissues to become contaminated by bacterial endotoxins and acids from the liquid present in the cavities of the implant.[17-20]

In a previous study, the gap formation observed in the Camlog K-series and Straumann synOcta systems was greater than that in the present study.[21] Neither the generation of the force nor the force coupling was different between the previous and the present studies, and therefore the apparent differences cannot be explained by the experimental methodology. The different gap widths could therefore most likely be due to changes in the manufacturers' portfolios since the prior study. In 2007, the Camlog J-series was tested, whereas the K-series was tested in our current investigation. Straumann's synOcta has also implemented product modifications in which secondary parts and the corresponding milling cylinder were changed. Within the past years, improvements in material science and implant technology have led to modifications in the implant design of many implant types. Regarding the IAC, a marked trend toward conical connections is obvious. However, there is still uncertainty about the significance of the type of IACs regarding the clinical long-term performance of implants, the importance in the development of peri-implantitis and the long-term stability of peri-implant hard and soft tissues.

Within the limits of the present in vitro study, the examination revealed that in both, conical (Figure 7) and butt connection (Figure 8A,B) implants, static loading caused greater dislocations of the abutments than the dynamic load in the identical experimental setup with the same force vector (200 N, 30°). However, to state superiority of a particular IAC further, especially clinical, studies of high scientific value are necessary.

5 | CONCLUSION

Dynamic loading of 100 N or more on IACs led to a cyclical opening and closing of gaps between the implant and the abutment. Such gaps, even when very small might allow a direct connection between the internal cavities of the implant and the peri-implant tissues, which could lead to contamination of the tissues by harmful liquids. In the present study, conical connections seemed to showed no or reduced formation of gaps during dynamic loading of 200 N compared with flat connections. However, also some conical connections presented a gap which seemed to depend on the platform diameter.

ACKNOWLEDGMENTS

The authors would like to thank Dr Jonas Lorenz for his technical assistance. Apart from the support of the authors' institution, this research did not receive any specific grant from funding agencies in the public, commercial, or not-for-profit sectors.

CONFLICT OF INTEREST

The authors declare that they have no potential conflicts of interest with the contents of this article.

ORCID

Paul Weigl http://orcid.org/0000-0001-7434-7988

REFERENCES

1. Krebs M, Schmenger K, Neumann K, Weigl P, Moser W, Nentwig GH. Long-term evaluation of ANKYLOS® dental implants, part I: 20-year life table analysis of a longitudinal study of more than 12,500 implants. *Clin Implant Dent Relat Res*. 2013;17:275-286.
2. Schropp L, Wenzel A. Timing of single implant placement and long-term observation of marginal bone levels. *Eur J Oral Implantol*. 2016;9:107-122.
3. Esposito M, Murray-Curtis L, Grusovin MG, Coulthard P, Worthington HV. Interventions for replacing missing teeth: different types of dental implants. *Cochrane Database Syst Rev*. 2007;4: CD003815.
4. Trulsson M. Sensory and motor function of teeth and dental implants: a basis for osseoperception. *Clin Exp Pharmacol Physiol*. 2005;32: 119-122.
5. Gross MD. Occlusion in implant dentistry. A review of the literature of prosthetic determinants and current concepts. *Aust Dent J*. 2008;53: 60-68.
6. Tey VHS, Phillips R, Tan K. Five-year retrospective study on success, survival and incidence of complications of single crowns supported by dental implants. *Clin Oral Implants Res*. 2017;28:620-625.
7. Blum K, Wiest W, Fella C, et al. Fatigue induced changes in conical implant-abutment connections. *Dent Mater*. 2015;31:1415-1426.
8. Lopes de Chaves E, Mello Dias EC, Sperandio M, Napimoga MH. Association between implant-abutment microgap and implant circularity to bacterial leakage: an in vitro study using tapered connection implants. *Int J Oral Maxillofac Implants*. 2018;33:505-511. https://doi.org/10.11607/jomi.5836
9. Wiest W, Zabler S, Rack A, et al. In situ microradioscopy and microtomography of fatigue-loaded dental two-piece implants. *J Synchrotron Radiat*. 2015;22:1492-1497.
10. Streckbein P, Streckbein RG, Wilbrand JF, et al. Non-linear 3D evaluation of different oral implant-abutment connections. *J Dent Res*. 2012; 91:1184-1189.

11. Rack A, Rack T, Stiller M, Riesemeier H, Zabler S, Nelson K. In vitro synchrotron-based radiography of micro-gap formation at the implant-abutment interface of two-piece dental implants. *J Synchrotron Radiat*. 2010;17:289-294.
12. Rack T, Zabler S, Rack A, Riesemeier H, Nelson K. An in vitro pilot study of abutment stability during loading in new and fatigue-loaded conical dental implants using synchrotron-based radiography. *Int J Oral Maxillofac Implants*. 2013;28:44-50.
13. Haraldson T, Carlsson GE, Dahlström L, Jansson T. Relationship between myoelectric activity in masticatory muscles and bite force. *Scand J Dent Res*. 1985;93:539-545.
14. Hagberg C. Electromyography and bite force studies of muscular function and dysfunction in masticatory muscles. *Swed Dent J Suppl*. 1986;37:1-64.
15. Kim HK, Heo SJ, Koak JY, Kim SK. In vivo comparison of force development with various materials of implant-supported prostheses. *J Oral Rehabil*. 2009;36:616-625.
16. Fretwurst T, Buzanich G, Nahles S, Woelber JP, Riesemeier H, Nelson K. Metal elements in tissue with dental peri-implantitis: a pilot study. *Clin Oral Implants Res*. 2016;27:1178-1186.
17. do Nascimento C, Pedrazzi V, Miani PK, Moreira LD, de Albuquerque RF Jr. Influence of repeated screw tightening on bacterial leakage along the implant-abutment interface. *Clin Oral Implants Res*. 2009;20:1394-1397.
18. do Nascimento C, Miani PK, Pedrazzi V, Muller K, de Albuquerque RF Jr. Bacterial leakage along the implant-abutment interface: culture and DNA checkerboard hybridization analyses. *Clin Oral Implants Res*. 2012;23:1168-1172.
19. do Nascimento C, Miani PK, Pedrazzi V, et al. Leakage of saliva through the implant-abutment interface: in vitro evaluation of three different implant connections under unloaded and loaded conditions. *Int J Oral Maxillofac Implants*. 2012;27:551-560.
20. Assenza B, Tripodi D, Scarano A, et al. Bacterial leakage in implants with different implant-abutment connections: an in vitro study. *J Periodontol*. 2012;83:491-497.
21. Zipprich H, Weigl P, Lange B, Lauer H-C. Erfassung, Ursachen und Folgen von Mikrobewegungen am Implantat-Abutment-Interface. *Implant Dent*. 2007;15:31-46.

SUPPORTING INFORMATION

Additional supporting information may be found online in the Supporting Information section at the end of the article.

How to cite this article: Zipprich H, Weigl P, Ratka C, Lange B, Lauer H-C. The micromechanical behavior of implant-abutment connections under a dynamic load protocol. *Clin Implant Dent Relat Res*. 2018;1–10. https://doi.org/10.1111/cid.12651